Local vibrational properties of GaAs studied by extended X-ray absorption fine structure

S. I. Ahmed, G. Aquilanti, N. Novello, L. Olivi, R. Grisenti et al.

Citation: J. Chem. Phys. **139**, 164512 (2013); doi: 10.1063/1.4826629
View online: http://dx.doi.org/10.1063/1.4826629
View Table of Contents: http://jcp.aip.org/resource/1/JCPSA6/v139/i16
Published by the AIP Publishing LLC.

Local vibrational properties of GaAs studied by extended X-ray absorption fine structure

S. I. Ahmed,[1,a)] G. Aquilanti,[1] N. Novello,[1] L. Olivi,[1] R. Grisenti,[2] and P. Fornasini[2,b)]
[1]*Elettra - Sincrotrone Trieste S.C.p.A., S.S. 14, 34149 Basovizza, Trieste, Italy*
[2]*Dipartimento di Fisica, Università degli Studi di Trento, I-38123 Povo, Trento, Italy*

(Received 28 August 2013; accepted 9 October 2013; published online 30 October 2013)

Extended X-ray absorption fine structure (EXAFS) has been measured at both the K edges of gallium and arsenic in GaAs, from 14 to 300 K, to investigate the local vibrational and thermodynamic behaviour in terms of bond expansion, parallel, and perpendicular mean square relative displacements and third cumulant. The separate analysis of the two edges allows a self-consistent check of the results and suggests that a residual influence of Ga EXAFS at the As edge cannot be excluded. The relation between bond expansion, lattice expansion, and expansion due to anharmonicity of the effective potential is quantitatively clarified. The comparison with previous EXAFS results on other crystals with the diamond or zincblende structure shows that the values of a number of parameters determined from EXAFS are clearly correlated with the fractional ionicity and with the strength and temperature interval of the lattice negative expansion. © *2013 AIP Publishing LLC*. [http://dx.doi.org/10.1063/1.4826629]

I. INTRODUCTION

The structural and vibrational properties of crystals are generally accounted for by considering the full crystal potential energy, typically within the Born von Kármán approach.[1] Experimental probes such as X-ray or neutron elastic and inelastic scattering are sensitive to average structural and dynamical properties: lattice parameters, uncorrelated atomic displacement parameters, normal modes dispersion, and so on. Extended X-ray absorption fine structure (EXAFS) is a short-range probe and gives complementary information on local properties, such as the correlation of atomic motion and the bond thermal expansion.[2,3] The possibility of probing the local structural and dynamical properties and comparing them with the average properties, in addition to its fundamental interest, is relevant for getting a deeper understanding of differences and similarities between nano-structured and bulk materials.

The differences between local and average structural properties can be accounted for as effects of atomic vibrations. The first pioneering works on the effects of atomic vibrations on EXAFS[4,5] focussed their attention on the interpretation of the Debye-Waller exponent within the harmonic approximation in terms of the parallel mean square relative displacement (MSRD). The relevance of asymmetry was early recognised,[6] and the cumulant expansion method[7,8] proved to be particularly suitable for treating relatively weak thermal disorder. More recently, the difference between the thermal expansions measured by EXAFS and by Bragg diffraction in crystals was experimentally detected, leading to the evaluation of the perpendicular MSRD; the role of the third cumulant was clarified too.[9,10]

All these findings contributed to increase the accuracy of EXAFS results and to refine their interpretation. They opened new perspectives for the understanding of phenomena connected to the local vibrational dynamics, such as negative thermal expansion[11,12] and isotopic effects.[13]

GaAs is widely employed in the manufacture of electronic and optoelectronic devices, both in bulk form and as nanoparticles and nanowires. To our knowledge, the last EXAFS study of thermal properties of bulk GaAs dates back to the 1990s and is limited to the investigation of the parallel MSRD in the temperature range from liquid nitrogen to room temperature.[14] This work presents new EXAFS measurements on GaAs, performed in a temperature range extended down to 14 K, in order to determine the bond thermal expansion and the MSRDs, both parallel and perpendicular, as well as the third cumulant and its influence on the bond expansion.

The aims of this work are many.

(a) A deeper understanding of EXAFS of bulk GaAs can contribute to increase the accuracy of investigations on nanoparticles, nanotubes, heterostructures based on GaAs.
(b) EXAFS gives original information on the local vibrational dynamics, whose reproduction is a quite unique benchmark for theoretical calculations, including the phase relations between eigenvectors of the dynamical matrix and the anharmonicity contributions.[15]
(c) In recent years, a number of crystals with the diamond-zincblende structure, affected by negative thermal expansion (NTE) at low temperatures, has been investigated: Ge,[9] CdTe,[12] CuCl,[16] InP.[17] The results suggest that a correlation exists between the bond ionicity, the NTE properties and some of the parameters determined from EXAFS analysis. The results from GaAs add new information for an intermediate value of ionicity and

a)Permanent address: Ain Shams University, Cairo, Egypt.
b)Author to whom correspondence should be addressed. Electronic mail: paolo.fornasini@unitn.it

can contribute to a more quantitative evaluation of the correlations.

(d) The possibility of measuring EXAFS at both the Ga and As K edges allows a self-consistent evaluation of the experimental accuracy of the EXAFS results. In a previous study on GaAs, a good agreement was found for the parallel MSRDs determined from the two edges.[14] Recently, an investigation based on EXAFS measurements at both Cd and Te K edges in CdTe has shown that a very good agreement can be obtained also for the first and third cumulants and for the perpendicular MSRD.[12,18] The case of GaAs is, however, technically more delicate: while the energy difference between the Cd and Te K edges is 5100 eV, the energy difference between the Ga and As K edges is 1500 eV, corresponding to a photo-electron wavevector range of about 19.3 $Å^{-1}$. It is of interest to evaluate the influence of the residual Ga EXAFS on the structural parameters determined from the As EXAFS.

Experimental details and data analysis procedures are summarized in Secs. II and III. The temperature dependence of the first-shell first four cumulants and perpendicular MSRD and of the outer shells second cumulants is presented in Sec. IV. The discussion of Sec. V is focussed on the leakage of Ga EXAFS on the As EXAFS, on the relation between the different thermal expansions measured by EXAFS and Bragg diffraction and on the comparison with other diamond-zincblende crystals. Section VI is dedicated to conclusions.

II. EXPERIMENT

Transmission EXAFS measurements have been performed on GaAs powders 99.9999% pure (from STREM) at the XAFS beamline of Elettra in Trieste, Italy.[19] The electron energy and the average current were 2 GeV and 300 mA, respectively. The X-ray beam was monochromatized by two silicon crystals with flat (111) parallel reflecting faces; the harmonics influence was reduced by reflection from a Pt-coated mirror.

The samples were prepared as pellets by mixing 0.02 g of GaAs with 0.20 g of graphite fine powder; a few ethanol drops were added during the mixing to increase the homogeneity. The sample homogeneity was checked by examining the distribution of the transmitted X-rays on a phosphorus screen behind the sample, as well as by scanning the sample using narrow vertical and horizontal collimating slits. The measurements were performed with the X-ray beam impinging on the largest homogeneous part in the middle of the sample.

The incoming and outgoing photon fluxes were measured by two ionization chambers filled with krypton gas, at pressures of 140 and 500 mbar, respectively. A second pellet of GaAs was inserted between the second and the third ionization chambers at ambient conditions to serve as a reference for energy calibration.

The sample was mounted in a liquid-He cryostat. A thermocouple (chromel-gold/iron 0.07%) was fixed to the cryostat cold finger, at a distance of about 1 mm from the pellet, to monitor its actual temperature. The temperature was varied in the interval from 14 to 350 K, at 25 or 50 K steps. At each temperature, three spectra were recorded for each edge.

The edge jump $\Delta\mu x$ was about 1.06 at the Ga K edge (10 367 eV) and 0.97 at the As K edge (11 867 eV). The energy of the incident X-rays was scanned in the ranges $E = 10\,130$–$11\,745$ eV (for Ga) and $E = 11\,627$–$13\,393$ eV (for As), with a ΔE step varying from 0.2 eV in the near-edge region to 5 eV at the end of the spectra, in order to obtain a uniform wavevector step $\Delta k = 0.025$ Å in the EXAFS region.

III. DATA ANALYSIS

The extraction of the EXAFS signals $\chi(k)$ from the experimental spectra has been performed according to a well established procedure.[16,18] For each of the two sets of measurements (Ga and As edges), the values of the photoelectron wave-vector k were calculated with respect to an edge energy conventionally set at the maximum of the first derivative of one of the low-temperature spectra, chosen as reference. The energy axes of all other spectra were then shifted to achieve the best superposition with the reference spectrum in the edge region and the edge energy of each spectrum was determined accordingly. The weighted EXAFS functions $k^2\chi(k)$ at the Ga and As edges are compared for selected temperatures in Figure 1. The Ga EXAFS cannot be studied beyond $k_{max} \simeq 19\,Å^{-1}$ due to the onset of the As edge. Correspondingly, the As EXAFS is expected to be slightly contaminated by the high-k tail of the Ga EXAFS.

The k-weighted EXAFS signals $k^3\chi(k)$ have been multiplied by a Gaussian window and Fourier transformed from $k_{min} = 2$ to $k_{max} = 18.6\,Å^{-1}$ and from $k_{min} = 2.4$ to $k_{max} = 18.3\,Å^{-1}$ for Ga and As EXAFS, respectively. The Fourier transforms for the Ga and As edges are compared in Figure 2 for selected temperatures. The peak centered at about 2.15 Å is due to the first-shell single scattering (SS) contribution (4 atoms at 2.448 Å). The structure between about 3.1 Å and 4.9 Å is due to the superposition of SS contributions from the second and third shells (12 atoms at 3.997 Å and 12 atoms at 4.687 Å, respectively) as well as to non-negligible non-collinear multiple scattering (MS) contributions.

To obtain quantitative results, the EXAFS signals have been parametrized in terms of the leading cumulants of the

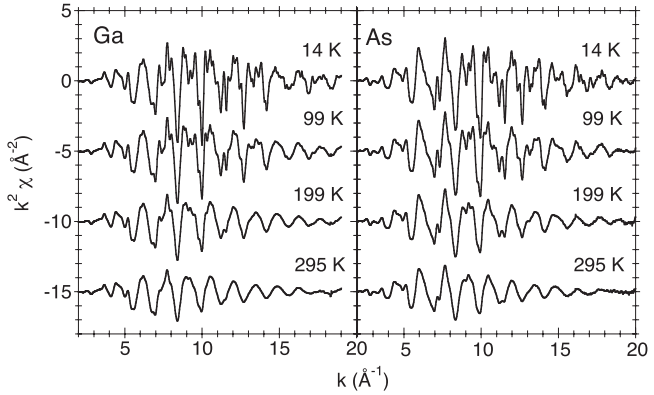

FIG. 1. EXAFS functions $k^2\chi(k)$ at the K edge of Ga (left) and As (right) in GaAs at some selected temperatures.

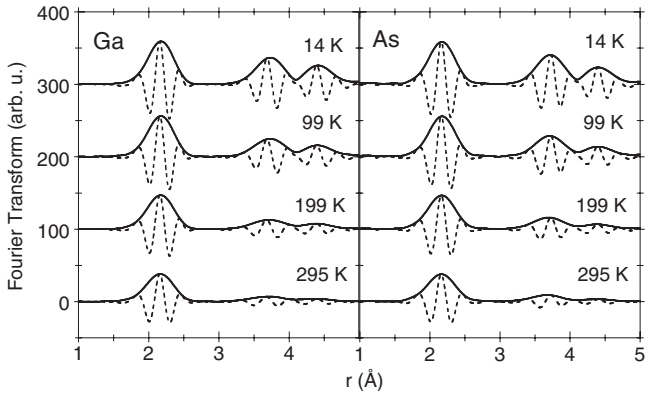

FIG. 2. Fourier transforms of the EXAFS functions at the K edge of Ga (left) and As (right) in GaAs at some selected temperatures: imaginary part (dashed lines) and moduli (continuous lines).

distributions of inter-atomic distances,[7] and two different analysis procedures have been carried out.[10,16]

As a first procedure, the *ratio method*[7,20,21] has been utilized for the first coordination shell, whose contribution can be neatly isolated (Figure 2) and where MS effects are absent. For each of the two sets of measurements (Ga and As edges), the first-shell EXAFS signals have been obtained by Fourier back-transform of the corresponding peaks in *r*-space (Fig. 2), and the phases and amplitudes have been separately analysed, taking the lowest temperature spectrum as reference. The ratio method gives the relative values $\delta C_n'$ of the leading cumulants of an effective distribution[7] $P(r,\lambda) = \rho(r)e^{-2r/\lambda}/r^2$, where $\rho(r)$ is the real distribution of distances and λ is the photoelectron mean free path. The cumulants of the real distribution, C_n^*, have been derived from the cumulants of the effective distribution, C_n', according to the recursion formula of Ref. 16; the electron mean free path was set to the value $\lambda(k) = 9 \pm 3$ Å. The difference between the cumulants of the real and effective distributions is significant only for the first cumulant. The criteria for evaluation of the cumulants accuracies is discussed in Ref. 18.

In the second procedure, backscattering amplitudes, phase shifts and inelastic terms have been calculated by using the FEFF6 code[22,23] and a nonlinear best-fit of theoretical to experimental spectra has been performed by the IFEFFIT code[24] using the graphical interface Artemis.[25] For the first shell, this procedure allows a check of the ratio method results; for the outer shells, it reasonably takes into account both SS and MS contributions. The first shell signal has been fitted in *r*-space between 1.6 Å and 2.6 Å; the values of e_0 and S_0^2 were considered independent of temperature and a unique value was refined at all temperatures; relative values of the cumulants have been calculated with respect to the lowest temperature, to allow a direct comparison with the ratio method.

The signal of the first and of the outer shells has been globally fitted in *r*-space between 1.6 Å and 4.8 Å including the first, second, and third-shell SS paths and a MS triangular "path4" Ga_0–Ga_2–As_1 or As_0–As_2–Ga_1 for Ga or As EXAFS, respectively. Another MS "path3" Ga_0–As_1–As_1 or As_0–Ga_1–Ga_1, occurring at the same path-length as "path4" but with smaller amplitude, was neglected. While e_0 and S_0^2 were considered independent of temperature as before, S_0^2 was equal for all paths and four different values of e_0 were refined for the four different paths. The radius of the triangular MS "path4" was expressed in terms of the radii of the first and second SS paths as, $r_4 = r_1 + r_2/2$. The second cumulants of the triangular MS "path4" have been constrained to those of the first and second SS paths.

IV. RESULTS

A. First-shell bond expansion

The first cumulant is the average value of the real distribution of distances, $C_1^* = \langle r \rangle = \langle |\mathbf{r}_b - \mathbf{r}_a| \rangle$, where $\mathbf{r}_a$ and $\mathbf{r}_b$ are the vector positions of the absorber and backscatterer atoms, respectively. The temperature variation $\delta C_1^* = C_1^*(T) - C_1^*(14\ \mathrm{K})$ measured by EXAFS and corresponding to the bond expansion is shown in Figure 3: the agreement between the results from the ratio method (full circles) and the nonlinear fit (open circles) is very good for both edges.

The bond expansions δC_1^* measured from the Ga and the As edges are in a worse agreement with respect to what was previously found for CdTe, where the bond expansions were measured from the Cd and Te edges.[12] In both cases (CdTe and GaAs), the bond expansion δC_1^* from the low-energy edges (Cd and Ga, respectively) is regular, while the bond expansion from the high energy edges (Te and As, respectively) shows a bump around $T \simeq 100$ K. However, while the bump for the Te case is comparable with the uncertainty bars,[18] the bump for the As case is significantly larger and cannot be simply attributed to random fluctuations. A possible explanation for this behaviour is the leakage of the Ga EXAFS in the As EXAFS (see Sec. V).

In Figure 3, the temperature variation $\delta R_c = R_c(T) - R_c(14\,\mathrm{K})$ of the crystallographic distance $R_c = |\langle \mathbf{r}_b \rangle - \langle \mathbf{r}_a \rangle|$ proportional to the lattice expansion measured by dilatometric techniques is also shown: as one can see, there is a non-negligible discrepancy between the values of Novikova[27] from 28 to 348 K (open squares) and the values of Leszczynski *et al.*[28] from 10 to 295 K.

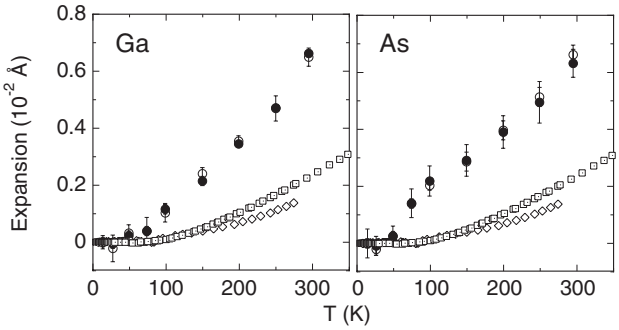

FIG. 3. Variation with temperature of the first-shell distance from EXAFS at the Ga (left panel) and As (right panel) K edges. Solid and open circles are relative values from the ratio method and from FEFFIT, respectively. The bond expansion evaluated from the lattice thermal expansion is represented by open squares (from Smith and White[26] and Novikova[27]) and by open diamonds (from Leszczynski *et al.*[28]).

As expected, the expansion measured by EXAFS is larger than the crystallographic expansion owing to the effect of thermal vibrations perpendicular to the bond[10,29]

$$\delta\langle r\rangle = \delta R_c + \frac{\delta\langle \Delta u_\perp^2\rangle}{2R_c}, \quad (1)$$

where $\langle \Delta u_\perp^2\rangle$ is the perpendicular mean square relative displacement (see below).

B. First-shell parallel MSRD

The second cumulant C_2^* is the variance $\sigma^2 = \langle (r - \langle r\rangle)^2\rangle$ of the real distribution of distances; it corresponds to the MSRD along the bond direction (for short, parallel MSRD):[4]

$$\sigma^2 = \langle \Delta u_\parallel^2\rangle = \langle (\hat{\mathbf{R}}\cdot\mathbf{u}_a)^2\rangle + \langle (\hat{\mathbf{R}}\cdot\mathbf{u}_b)^2\rangle - 2\langle (\hat{\mathbf{R}}\cdot\mathbf{u}_a)(\hat{\mathbf{R}}\cdot\mathbf{u}_b)\rangle, \quad (2)$$

where $\mathbf{u}_a$ and $\mathbf{u}_b$ are the instantaneous displacements of absorber and back-scatterer atoms, respectively, $\hat{\mathbf{R}}$ is the unit vector along the bond direction and $\Delta\mathbf{u} = \mathbf{u}_b - \mathbf{u}_a$.

Absolute values of the parallel MSRD have been evaluated by fitting an Einstein correlated model[30] to the relative values from the ratio method and from the nonlinear fit analysis and are shown in Fig. 4 as solid circles.

The best-fitting Einstein frequencies are slightly different for the two edges and for the different analysis methods. As one can see in Table I, the difference between the three analysis methods is larger for the As edge (up to 4%) than for the Ga edge (about 1%). On the other hand, the difference between the As and Ga edges for the ratio method is less than 0.2%. One reasonable explanation for this behaviour is the leakage of the Ga EXAFS in the As EXAFS, which was previously suggested to affect the phase of the EXAFS signal and be responsible for the slightly anomalous behaviour of the bond expansion at the As edge. The leakage effect on the EXAFS amplitudes is probably boosted, in the nonlinear fitting procedures, by the correlation of phase and amplitude parameters, which is weaker in the ratio method.

Assigning a larger weight to the results from the ratio method and from the Ga edge, we quote the average Einstein frequency and its standard uncertainty as $\nu_\parallel = 6.89 \pm 0.08$ THz. The Einstein frequency corresponds an effective bond-stretching force constant $k_\parallel = \mu(2\pi\nu_\parallel)^2 = 7.02 \pm 0.16$ eV/Å^2, where μ is the reduced mass.

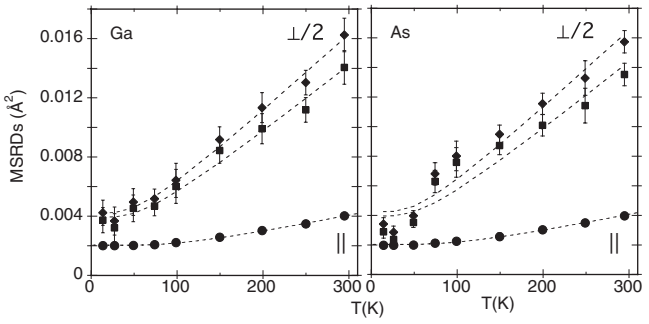

FIG. 4. Parallel MSRD $\langle \Delta u_\parallel^2\rangle$ (solid circles) and half perpendicular MSRD $\langle \Delta u_\perp^2\rangle/2$ (solid squares and diamonds refer to crystallographic distances from Novikova[27] and from Leszczynski *et al.*,[28] respectively). Dashed lines are best-fitting Einstein models. Left and right panels refer to Ga and As edges, respectively.

TABLE I. Einstein frequencies (in THz) best fitting the first-shell parallel MSRD.

Analysis method	Ga	As
Ratio method	6.83	6.84
Nonlinear fit, 1 path	6.88	7.05
Nonlinear fit, 4 paths	6.90	7.10

The value 6.89 ± 0.08 THz of the Einstein frequency is slightly smaller than the value 7.5 ± 0.5 THz quoted in a previous paper,[14] which was based on measurements performed only at and above 77 K at a first-generation synchrotron radiation source.

C. First-shell perpendicular MSRD

The perpendicular MSRD $\langle \Delta u_\perp^2\rangle$ is the projection of the total MSRD in the plane perpendicular to $\hat{\mathbf{R}}$ and is defined by[29]

$$\langle \Delta u_\perp^2\rangle = \langle \Delta u^2\rangle - \langle \Delta u_\parallel^2\rangle. \quad (3)$$

As usual,[10,12] the temperature dependence of $\langle \Delta u_\perp^2\rangle$ has been experimentally obtained from the difference between δC_1^* and δR_c, by inverting Eq. (1). In the present case, two significantly different crystallographic expansions have been quoted in the literature[27,28] (Fig. 3) and two different estimates of $\delta\langle \Delta u_\perp^2\rangle$ have been obtained accordingly.

Absolute values of $\langle \Delta u_\perp^2\rangle$ have been evaluated in both cases by fitting an Einstein correlated model to the relative values.[30] The results are shown in Fig. 4, where the half-values $\langle \Delta u_\perp^2\rangle/2$, corresponding to the projection along one direction (solid squares and diamonds), are compared with $\langle \Delta u_\parallel^2\rangle$ (solid circles). The temperature dependence of the perpendicular MSRD is more regular for the Ga edge than for the As edge, as a consequence of the bump observed in the bond expansion measured at the As edge.

The best-fitting Einstein frequencies $\nu_\perp$ for the perpendicular MSRDs and the corresponding effective force constants $k_\perp = \mu(2\pi\nu_\perp)^2$ are listed in Table II, together with the parameter $\xi = k_\parallel/k_\perp$ that measures the perpendicular to parallel anisotropy of relative displacements.[12,29]

TABLE II. Einstein frequencies $\nu_\perp$ and effective force constants $k_\perp$ best fitting the first-shell perpendicular MSRD and anisotropy parameter $\xi = k_\parallel/k_\perp$. The results from the crystallographic expansions of Leszczynski *et al.*[28] and of Novikova[27] are distinguished.

	Ga		As	
	28	27	28	27
$\nu_\perp$ (THz)	3.30 ± 0.03	3.54 ± 0.04	3.28 ± 0.03	3.52 ± 0.04
$k_\perp$ (eV/Å^2)	1.61 ± 0.03	1.85 ± 0.04	1.59 ± 0.03	1.86 ± 0.04
$\xi = k_\parallel/k_\perp$	4.36 ± 0.03	3.78 ± 0.03	4.41 ± 0.03	3.77 ± 0.03

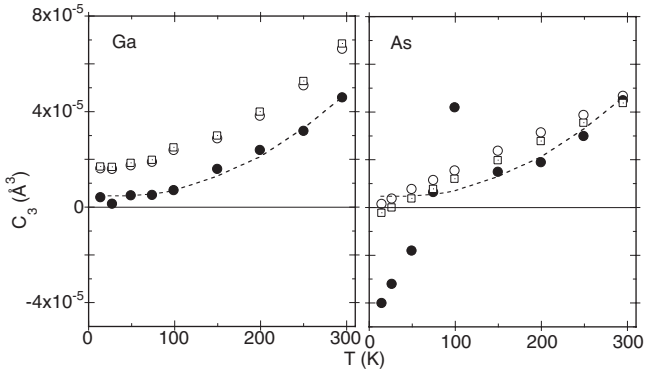

FIG. 5. Third cumulants obtained from Ga (left panel) and from As (right panel). The solid circles are results from the ratio method, fitted to a quantum perturbative model (dashed lines). The open circles and open squares are results from nonlinear fit including four and one scattering paths, respectively.

D. First-shell third cumulant

The third cumulant $C_3^* = \langle (r - \langle r \rangle)^3 \rangle$, which measures the asymmetry of the distribution of distances, is shown in Figure 5, where the results for the Ga and As edges and for the different analysis procedures are compared. The difference between Ga and As edges is immediately evident.

For the Ga edge (Fig. 5, left panel), absolute values C_3^* (full circles) have been evaluated by fitting the quantum perturbative model[31,32]

$$C_3^* \simeq -\frac{2\,k_3\sigma_0^4}{k_0}\,\frac{z^2+10z+1}{(1-z)^2} \tag{4}$$

to the relative values from the ratio method. In Eq. (4), $z = \exp(-\beta\hbar\omega_\parallel)$, $\omega_\parallel = \sqrt{k_\parallel/\mu}$, μ is the reduced mass and $\omega_\parallel$ is the Einstein angular frequency determined from the second cumulant. The value of the best-fitting third-order force constant is $k_3 = -3.94\,\text{eV/Å}^3$, and the zero Kelvin value is 0.45×10^{-5} Å^3. The values obtained by the nonlinear fitting procedures (open symbols in Figure 5) have the same temperature dependence as the values of the ratio method, consistent with the model of Eq. (4); the absolute values are however higher; the discrepancy could be due to residual structural disorder or to a slight inaccuracy of phase calculations.

The situation for the As edge is quite different (Fig. 5, right panel). Only the high-temperature data of the ratio method are consistent with the theoretical model determined from the Ga results (dashed line); the low-temperature data exhibit a completely different trend. Also the nonlinear fit results are significantly different, both in absolute and relative values, from the Ga results. This behaviour can be correlated with the anomalous behaviour of the bond expansion. The larger deviation from regularity found by the ratio method with respect to the nonlinear-fit can be attributed to the stronger sensitivity of the ratio method to the quality of data, in particular when tiny phase differences are considered.

E. First-shell fourth cumulant

The fourth cumulant C_4^* is shown in Figure 6, where the results from the ratio method for Ga and As edges are compared.

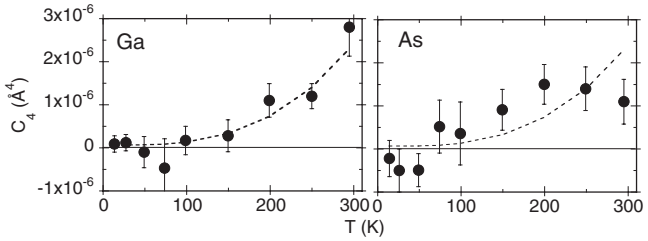

FIG. 6. Fourth cumulants obtained from Ga (left panel) and from As (right panel). The solid circles are results from the ratio method, fitted to a quantum perturbative model (dashed lines).

The Ga results (Fig. 6, left panel) are satisfactorily fitted to the quantum perturbative model[32]

$$\begin{aligned} C_4^* = &-\frac{12\,k_4\sigma_0^8}{\hbar\omega}\,\frac{z^3+9z^2+9z+1}{(1-z)^3} \\ &-\frac{144\,k_4\sigma_0^8}{k_BT}\,\frac{z^2}{(1-z)^4} \\ &+\frac{12\,k_3^2\sigma_0^{10}}{(\hbar\omega)^2}\,\frac{5z^3+109z^2+109z+5}{(1-z)^3} \\ &+\frac{720\,k_3^2\sigma_0^{10}}{\hbar\omega k_BT}\,\frac{z^2}{(1-z)^4} \end{aligned} \tag{5}$$

(dashed line) with a fourth-order force constant $k_4 = -3.96\,\text{eV/Å}^4$ and a zero point value 0.7×10^{-7} Å^4. The fourth cumulants from the As edge (Fig. 6, right panel) show a less regular behaviour, still compatible with the model (5) best-fitting the fourth cumulants of the Ga edge.

F. Outer shell results

As in previous similar works,[10,12] no results of sufficient resolution and accuracy could be obtained for the thermal expansion of single interatomic distances of the outer shells.

Accurate results have been obtained for the second cumulants (parallel MSRDs), whose temperature dependence is shown in Figure 7. Three pairs of atoms are involved: Ga–As for the first and the third shells of both Ga and As,

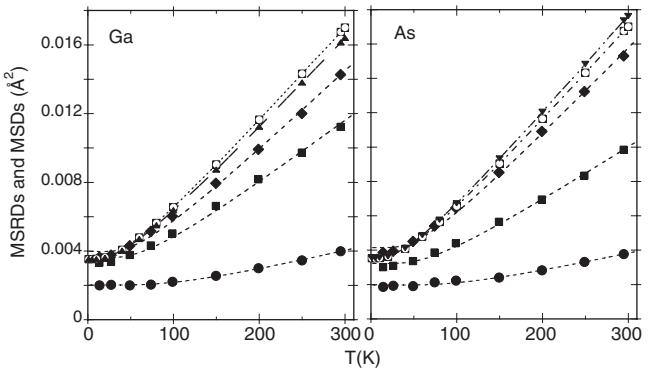

FIG. 7. Parallel MSRDs for the first three coordination shells of Ga (left panel) and of As (right panel): 1st shell (circles), 2nd shell (squares), 3rd shell (diamonds). Open squares, up triangles, and down triangles are the sums of uncorrelated MSDs from Ref. 33 for the three possible pairs: Ga–As, Ga–Ga, and As–As, respectively.

TABLE III. Einstein frequencies $\nu_\parallel$, effective force constants $k_\parallel$, and Debye temperatures Θ_D of the first three coordination shells determined from Ga and As EXAFS.

		$\nu_\parallel$ (THz)		$k_\parallel$ (eV/Å^2)		Θ_D (K)	
	Shell	Ga	As	Ga	As	Ga	As
1	Ga–As	6.86	6.96	6.96	7.16	401	403
2	Ga–Ga	4.02		2.30		231	
	As–As		4.18		2.68		240
3	Ga–As	3.52	3.37	1.823	1.68	201	193

Ga–Ga for the second shell of Ga, As–As for the second shell of As. The Einstein frequencies and the corresponding effective force-constants $k_\parallel$ are listed in Table III. The force constant of the As–As 2nd-shell distance is larger than the force constant of the Ga–Ga 2nd-shell distance. A similar behaviour was found for the Cd–Cd and Te–Te pairs in CdTe.[12] The expected agreement between the results of the separate analyses of the Ga and As EXAFS for the 3rd shell (Ga–As distance) is worse than in the case of CdTe. The last column of Table III lists the Debye temperatures of the best fitting Debye correlated model.

The sums of uncorrelated mean square displacements (MSD) $\langle(\hat{\mathbf{R}}\cdot\mathbf{u}_a)^2\rangle + \langle(\hat{\mathbf{R}}\cdot\mathbf{u}_b)^2\rangle$ are also shown in Figure 7; these values have been obtained from the Debye-Waller factors calculated by a shell model[33] best-fitting the experimental phonon dispersion curves. The MSD values are of help in evaluating the correlation effects, which decrease in going from the first to the third shell. By comparing Figure 7 with Figure 4 one can also appreciate that the correlation effect is much stronger for the parallel than for the perpendicular relative atomic motion.

V. DISCUSSION

A. Comparison of Ga and As edges

A non-negligible discrepancy has been observed between the results from the Ga and As edges, mainly concerning the phase of the signal. The first-shell bond expansion and the perpendicular MSRD from As are characterised by a bump in a temperature region around about 100 K (Figs. 3 and 4), and the third cumulant has a very irregular behaviour at low temperatures (Fig. 5). The corresponding quantities from Ga EXAFS exhibit a regular temperature dependence. A similar effect, although much weaker, was observed for CdTe;[12,18] in that case, the discrepancy between the results from Cd and Te EXAFS was consistent with the uncertainty bars. In the present case of GaAs the discrepancy is significantly larger than the uncertainty bars.

One possible cause of the discrepancy is the residual influence of the Ga EXAFS on the As EXAFS. The distance between the two edges corresponds to $\Delta k \simeq 19.3$ Å^{-1} (for CdTe, $\Delta k \simeq 36$ Å^{-1}).

To support this hypothesis, one can easily verify that the frequencies of the 1st, 2nd, and 3rd shell contributions to the Ga EXAFS, when extended beyond the As K edge, are comparable with the frequency of the 1st-shell contribution to the As EXAFS for $k \geq 5$ Å^{-1}. Besides, the amplitude of the Ga EXAFS contributions in the As EXAFS region, reduced by the decreasing backscattering amplitude and the Debye-Waller factor, is of the order of 1% with respect to the As EXAFS, not negligible when tiny effects of phase variations are sought.

The comparison between EXAFS at different edges is in principle a valuable check of self-consistency of experimental results.[18] The case of GaAs suggests, however, that such a check should be considered quite cautiously even for relatively distant edges when resolutions (and accuracies) better than 10^{-3} Å are sought for relative distances.

B. Bond expansion and crystallographic expansion

The difference between bond expansion δC_1^* and the crystallographic expansion δR_c, according to Eq. (1), allows the evaluation of the perpendicular MSRD.[10,12] The accuracy of this procedure is affected by the accuracies of the involved experimental techniques; for GaAs, the crystallographic thermal expansions of Novikova[27] and of Leszczynski *et al.*[28] lead to two different estimates of perpendicular MSRD (Fig. 4). In the following, we refer to the results of Novikova,[27] which are part of an extensive work of thermal expansion measurements on many crystals; the results of Novikova had been previously considered also for CdTe.[12]

EXAFS and crystallographic expansions have been independently represented in Fig. 3, where both expansions are zero for $T = 0$ K. Once the absolute values of the perpendicular MSRD and of the second and third cumulant have been evaluated, one can attempt to gain a better quantitative evaluation of the difference between EXAFS and crystallographic expansions.

Let R_0 be the distance between absorber and backscatterer atoms, ideally frozen at their equilibrium positions. The bond distance measured by the first EXAFS cumulant $\langle r\rangle$ can be expressed, by simple considerations of vibrational dynamics,[29] as

$$\langle r\rangle \simeq R_0 + \langle\Delta u_\parallel\rangle + \frac{\langle\Delta u_\perp^2\rangle}{2R_0}\,, \tag{6}$$

where $R_0 + \langle\Delta u_\parallel\rangle = R_c$ is the crystallographic distance. Note that $\langle\Delta u_\parallel\rangle$ is different from zero even at $T = 0$ K. By measuring the crystallographic distance R_c at different temperatures, one can obtain the relative crystallographic expansion $\delta R_c = R_c(T) - R_c(0)$ but not the absolute expansion corresponding to $\langle\Delta u_\parallel\rangle$. The bond and crystallographic expansions $\delta\langle r\rangle$ and δR_c are connected by Eq. (1).

Alternatively, the bond distance can be expressed, within the one-dimensional model,[29] as

$$\langle r\rangle \simeq R_0 + a + \delta R_\Phi\,, \tag{7}$$

where $a = -3\,k_3C_2/k_\parallel$ is the absolute expansion solely due to the asymmetry of the effective pair potential, as evaluated by a quantum perturbative approach,[31] and δR_Φ is the contribution to expansion due to a rigid shift of the effective pair potential.[10,34]

The quantity a, evaluated from the experimental values of the second cumulant C_2 and of the force constants $k_\parallel$ and

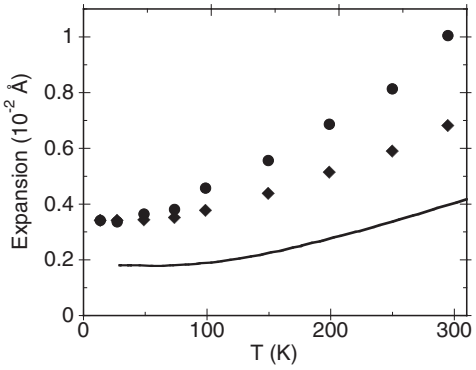

FIG. 8. Bond distance $\langle r \rangle$ (solid circles), thermal expansion due to the asymmetry of the effective pair potential (diamonds) and crystallographic distance (continuous line) evaluated with respect to the hypothetic distance of atoms frozen at their equilibrium positions at $T = 0$ K.

k_3, is shown by diamonds in Fig. 8. If one assumes $\delta R_\Phi = 0$ for $T = 0$ K in Eq. (7), the zero of the vertical axis in Fig. 8 corresponds to the equilibrium distance R_0 (unknown), and the bond expansion $\delta\langle r \rangle$ measured by the variation of the first EXAFS cumulant δC_1^* can be considered as beginning at the value of a for $T = 0$ K (solid circles in Fig. 8).

The difference of the temperature dependencies δa and $\delta\langle r \rangle$ confirms that the bond expansion measured by the variation of the first cumulant cannot be accounted for solely by the asymmetry of the effective pair potential, as experimentally found in a number of different cases.[9,10,12,16,35] These findings justify the assumption of a temperature dependent rigid shift of the effective pair potential δR_Φ in Eq. (7).

The presence of the rigid shift has been confirmed for Cu by path-integral Monte-Carlo simulations[34] and for Ge by Molecular Dynamics simulations.[36] In both cases, the simulations further show that for the second and outer shells the contribution of the potential asymmetry to the inter-atomic distance thermal expansion is much smaller than for the first shell, and the contribution of the effective potential shift is predominant.

It has to be here remembered that the effective pair potential connected to the distribution of interatomic distances sampled by EXAFS is different from the (temperature independent) single pair potential; the effective pair potential depends on the statistically averaged influence of all the other atoms.[37]

Once the bond distance $\langle r \rangle$ has been represented with respect to R_0 in Fig. 8, one can take advantage of the absolute values obtained for the perpendicular MSRD to arrange the crystallographic distance $R_c = \langle r \rangle - \langle \Delta u_\perp^2 / 2R_0$ on the same scale (continuous line, from Ref. 27). The difference between the EXAFS distance and the crystallographic distance at $T = 0$ K is about 1.6×10^{-3} Å, intermediate between the values 1.5×10^{-3} and 1.8×10^{-3} Å found for Ge and CdTe, respectively.[18] Again at $T = 0$ K one can evaluate $\langle \Delta u_\parallel \rangle = R_c - R_0 \simeq 1.8 \times 10^{-3}$ Å.

C. Comparison of zincblende structures

Let us now compare the present results for GaAs with the results previously obtained for other crystals with the diamond or zincblende (sphalerite) structure: Ge,[9,13] CdTe,[12] and CuCl.[16]

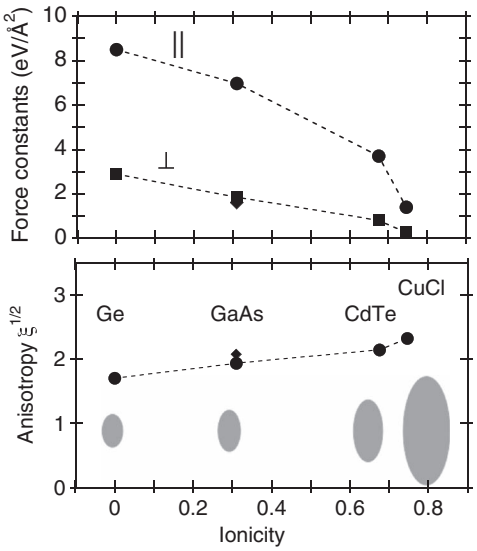

FIG. 9. Parallel and perpendicular effective force constants $k_\parallel$ and $k_\perp$ (upper panel) and anisotropy parameter $\xi^{1/2} = (k_\parallel / k_\perp)^{1/2}$ (lower panel) as a function of ionicity for a number of different crystals sharing the diamond-zincblende structure. The diamonds for GaAs are the values obtained from the crystallographic expansion of Leszczynski *et al.*[28] The dashed lines are a guide for eyes. The in-scale two-dimensional projections of the ellipsoids of relative displacements at $T = 300$ K are sketched at the bottom of the lower panel.

When comparing the vibrational properties of different isostructural compounds, it is preferable to refer to the effective force constants rather than to the frequencies. Actually, the frequencies $\nu = (k/\mu)^{1/2}/2\pi$ represent the response of the pair of atoms to the interaction force, and depend on the inertia, measured by the reduced mass.

The parallel and perpendicular effective force constants best-fitting the temperature dependence of the parallel and perpendicular MSRDs, $k_\parallel$ and $k_\perp$, respectively, are plotted in the upper panel of Fig. 9 as a function of the fractional ionic character.[38] Both effective force constants decrease when the ionicity increases, indicating the progressive loosening of the resistance against bond stretching and bond bending, respectively. Correspondingly, the extent of relative thermal motion increases in both parallel and perpendicular directions with respect to the bond. The different values of the two effective force constants $k_\parallel$ and $k_\perp$ and their different dependencies on ionicity imply that the distributions of relative displacements are not isotropic. While the distributions of the single atom displacements are spherical in all the diamond-zincblende crystals, for symmetry reasons, the ellipsoids of relative displacements are disc-shaped, the anisotropy depending on the degree of ionicity.

A previously introduced measure of the anisotropy of relative displacements,[12,39]

$$\xi = \frac{k_\parallel}{k_\perp} = \lim_{T \to \infty} \frac{\langle \Delta u_\perp^2 \rangle}{2\langle \Delta u_\parallel^2 \rangle} \tag{8}$$

refers to the asymptotic ratio of the parallel and perpendicular MSRDs. A more direct insight is given by the square root of ξ, which is connected with the standard deviations σ of the

ellipsoids:

$$\xi^{1/2} = \lim_{T\to\infty} \sigma_\perp/\sigma_\parallel . \quad (9)$$

The anisotropy parameters $\xi^{1/2}$ are shown in the lower panel of Fig. 9. Their values are significantly larger than one (isotropy case) and increase when the ionicity increases. A pictorial comparison of the relative extent of the ellipsoids of relative displacements for $T = 300$ K is given at the bottom of the lower panel in Fig. 9.

For copper,[10] the anisotropy parameter is $\xi^{1/2} = 1.1$. The larger anisotropy of the diamond-zincblende crystals with respect to fcc copper can be qualitatively understood in terms of their low coordination number and open structure, which favours the relative vibrations of neighbouring atoms perpendicular to the bond direction.

The experimental values of the asymptotic ratios $\lim_{T\to\infty} \langle \Delta u_\perp^2 \rangle / \langle \Delta u_\parallel^2 \rangle = 2\xi$ are 2.2 for Cu, 5.78 for Ge, 7.44 for GaAs, and 9.15 for CdTe, in good agreement with the values calculated *ab initio* by Vila *et al.*,[15] 2.36 for Cu at 500 K and 7.2 for diamond lattices at 600 K.

The effective force constants $k_\parallel$ and $k_\perp$ should not be confused with the force constants of lattice dynamical models. A comparison of the EXAFS effective force constants with the force constants k_r and k_θ of a valence force field (VFF) model[40] that Martin[38] extended to ionic ZB systems has been performed for Ge, CdTe, and CuCl in Ref. 12. For Ge, $k_\parallel$ is 12% larger than k_r and $k_\perp$ is about six times larger than k_θ. When the ionicity increases, the decrease of $k_\parallel$ is stronger than the decrease of k_r, and $k_\perp$ is always about six times larger than k_θ.

The third order force constant k_3, obtained by best fitting Eq. (4) to the temperature dependence of the third cumulant, exhibits a regular trend as a function of ionicity (Fig. 10, top panel). The third-order force constant quantifies the first anharmonic correction to the effective pair potential. The decrease of $|k_3|$ is accompanied by an increase of the third cumulant, say of the asymmetry of the distribution of distances, when the ionicity increases. This apparent contradiction can be solved by considering the relation between k_3 and the third cumulant, Eq. (4). The classical approximation $C_3 = -(6k_3/k_\parallel^3)(k_B T)^2$ (Refs. 20 and 41), which significantly differs from the quantum expression (4) only at very low temperatures, shows that the third cumulant depends proportionally on k_3 and inversely on the third power of $k_\parallel$. In all considered systems, the decrease of k_3 is accompanied by a decrease of $k_\parallel$, which explains the third cumulant increase.

The asymmetry of the distribution of distances is measured by the skewness parameter $\beta = C_3/C_2^{3/2}$, which is a temperature dependent quantity. As one can see in the bottom panel of Fig. 10, the asymmetry increases when the ionicity increases.

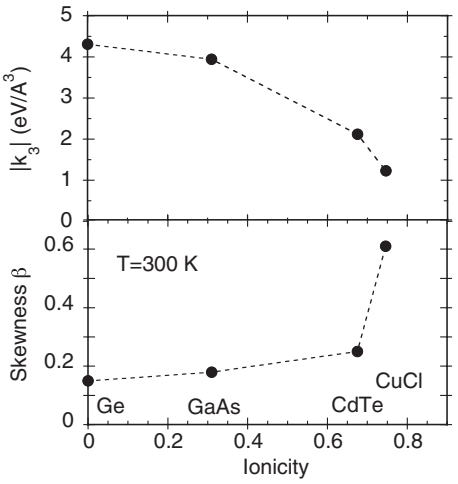

FIG. 10. Magnitude of the third-order effective force constant $|k_3|$ (top panel) and skewness parameter $\beta = C_3/C_2^{3/2}$ evaluated at $T = 300$ K (bottom panel) as a function of ionicity for a number of different crystals sharing the diamond-zincblende structure.

D. Negative thermal expansion

The tetrahedral semiconductors here considered undergo isotropic NTE within limited low-temperature intervals.[42] The NTE strength, measured by the minimum value of the expansion coefficient and by the width of the NTE temperature interval, increases with increasing ionicity.

According to the Barron's phenomenological model,[43] the lattice expansion measured by dilatometry or Bragg scattering is the sum of a positive bond stretching contribution due to the anharmonicity of the effective pair potential and a negative contribution due to tension effects. When tension effects prevail over bond stretching, the solid contracts upon heating.

The direct measurement by EXAFS of the bond expansion $\delta\langle r \rangle$ and, by comparison with crystallographic expansion, the evaluation of the perpendicular MSRD $\langle \Delta u_\perp^2 \rangle$ correspond to experimentally disentangling the contributions of bond stretching and tension effects to the lattice thermal expansion, as per Eq. (1).

Tension effects are particularly effective in crystals where linear A–B–A links are present, such as framework structures or delafossite structures;[39,44,45] in these systems, tension effects are monitored both by the anisotropy of the atom B vibrations and by the stronger anisotropy of the relative vibrations of the A–B pair. In crystals with the diamond-zincblende structure, the atomic vibrations are isotropic for symmetry reasons; only the relative vibrations of nearest-neighbour pairs evaluated from EXAFS are anisotropic, the anisotropy increasing with the ionicity and with the strength of NTE (Fig. 9).

E. Outer shells Debye-Waller factors

The parallel MSRDs for the first three coordination shells are shown in Fig. 7. As expected, the parallel MSRDs increase when the inter-atomic distance increases from first to third shell.

A quantitative assessment of the different behaviour of the different shells, as well as of the agreement between Ga and As EXAFS, can be obtained from the values of the parallel effective force-constants $k_\parallel$ that are listed in Table III. The agreement between the Ga and As EXAFS is good for the 1st

shell (Ga–As distance). The force constant of the As–As 2nd-shell is about 15% larger than the force constant of the Ga–Ga 2nd-shell. A similar behaviour was found for CdTe,[12] where the force constant of the Te–Te 2nd-shell is about 30% larger than the force constant of the Cd–Cd 2nd-shell. A discrepancy of 8% is present for the Ga and As third shell force constants, which refer to the same Ga–As coordination (a much smaller discrepancy was found for CdTe).

The temperature dependence of the parallel MSRDs have been fitted to Debye correlated models. The Debye temperatures for the different coordination shells, listed in Table III, are significantly different, varying from about 400 K for the first shell to about 200 K for the third shell. The specific heat Debye temperature[46] is $\Theta_D = 344$ K at 0 K and about 370 K above 100 K. For copper, the Debye temperatures of first, third, and fourth shells are instead very similar (in the range from 322 to 329 K) and the Debye temperature of the second shell is only slightly smaller (291 K)[10] in good agreement with the Debye temperatures of specific heat and of X-ray diffraction (315 and 313 K, respectively).

The Debye model is based on a more realistic approximation to the density of vibrational states than the Einstein model. The difference between the two models can, however, be barely appreciated when fitting to experimental data, in view of the data uncertainty and of the anharmonicity contributions. The Debye model is useful for monatomic Bravais crystals, such as copper, for which the Debye temperature is very similar for the different coordination shells and comparable with the Debye temperatures from other techniques. For non-Bravais crystals, such as Ge or GaAs, the Einstein model is recommended for its simplicity and for the possibility of connecting the Einstein frequencies to the effective force constants that measure the effective strength of the bond between absorber and backscatterer atoms.

By comparing the parallel MSRDs with the sum of the single atom MSDs, one can evaluate the degree of correlation for the different coordination shells. The extent of correlation can be measured by a dimensionless normalised function of temperature defined as[47,48]

$$\phi_{\parallel}(T) = \frac{\langle(\hat{R}\cdot\vec{u}_b)^2\rangle + \langle(\hat{R}\cdot\vec{u}_a)^2\rangle - \langle\Delta u_{\parallel}^2\rangle}{2[\langle(\hat{R}\cdot\vec{u}_b)^2\rangle\langle(\hat{R}\cdot\vec{u}_a)^2\rangle]^{1/2}}. \qquad (10)$$

A value $\phi_{\parallel} = 0$ corresponds to a completely uncorrelated motion of the two atoms. Values $\phi_{\parallel} = 1$ and $\phi_{\parallel} = -1$ correspond to atomic motions perfectly in phase and in opposition of phase, respectively.

The values $\phi_{\parallel}$ at $T = 300$ K for the different shells of GaAs are listed in Table IV and compared with the values for other systems. The reliability of the ϕ values depends not only on the accuracy of EXAFS results, but also on the accuracy of the uncorrelated MSDs values. For Cu and CdTe, good quality recent experimental MSD data are available in the literature.[49–51] For GaAs and Ge we refer here to theoretical calculations.[33,52]

In spite of the difficulty in assessing the accuracy of experimental and theoretical data, some qualitative properties are evident in Table IV. The first-shell parallel correlation is much stronger in tetrahedral semiconductors than in copper.

TABLE IV. Correlation functions $\phi_{\parallel}$ and $\phi_{\perp}$ evaluated at $T = 300$ K for different crystals. For the 2nd shells of GaAs and CdTe, the first and second lines refer to the lightest pair (Ga–Ga and Cd–Cd) and to the heaviest pair (As–As and Te–Te), respectively.

	Shell	Cu	Ge	GaAs	CdTe
$\phi_{\parallel}$	1	0.46	0.77	0.76	0.83
	2	0.14	0.18	0.32	0.33
				0.44	0.41
	3	0.24	0	0.14	0.27
	4	0.23			
$\phi_{\perp}$	1	0.36	0.37	0.18	0.13

This difference can be attributed to the difference between the totally or partially covalent bonds of tetrahedral semiconductors and the metallic bond of copper. The correlation is instead comparable for the outer shells.

For the first shell, one can evaluate a perpendicular correlation $\phi_{\perp}$ by substituting $\langle\Delta u_{\perp}^2\rangle/2$ for $\langle\Delta u_{\parallel}^2\rangle$ in Eq. (10). The $\phi_{\perp}$ values at 300 K are listed in the last line of Table IV. The perpendicular correlation is only slightly larger than the parallel correlation for Cu; correspondingly, the anisotropy is very small. The perpendicular correlation of Ge is significantly smaller than the parallel correlation; this explains the larger anisotropy of Ge. The similarity of perpendicular correlations of Cu and Ge suggests that the smaller lateral rigidity of the metallic bond with respect to the covalent bond is compensated by the closer packing of the fcc structure. The reduction of perpendicular correlation in going from Ge to GaAs to CdTe is an effect of the increasing ionicity.

VI. CONCLUSIONS

Temperature dependent EXAFS measurements have been performed on GaAs at both the Ga and As K edges, from 14 to 300 K. The first cumulants of the nearest-neighbours distance distribution are in satisfactory agreement; the residual discrepancy between Ga and As EXAFS suggests that the influence of the Ga EXAFS on the As EXAFS is not negligible.

The bond expansion measured by EXAFS, the crystallographic expansion and the contribution to expansion due to the asymmetry of the effective potential are significantly different. The effect of perpendicular vibrations on nearest-neighbours thermal expansion has been estimated as 1.6×10^{-3} Å at 0 K for GaAs.

The comparison with previous EXAFS results for other crystals with the diamond-zincblende structure shows that a correlation exists between the fractional ionic character and a number of parameters, such as the parallel and perpendicular force constants, the anisotropy of relative vibrations and the skewness parameter.

By EXAFS measurements one can disentangle the contributions to lattice expansion due to bond stretching and to tension effects. The intensity of perpendicular relative vibrations and the anisotropy of relative thermal ellipsoids are correlated to the strength of negative thermal expansion.

The calibration of EXAFS measurements and analyses on model crystals such as bulk GaAs should be of benefit to EXAFS studies of more complex systems, such as nanostructures, interfaces, random ternary alloys.

ACKNOWLEDGMENTS

We acknowledge Sincrotrone Trieste (Elettra) for provision of synchrotron radiation facilities. The EXAFS measurements have been done during in-house research time. The Elettra staff is grateful to R. Natali, M. Minicucci, and A. Di Cicco from the University of Camerino for installation and optimization of the He cryostat done through a collaboration agreement. S. I. Ahmed is grateful to the TRIL programme at ICTP for financial support.

[1]M. Born and K. Huang, *Dynamical Theory of Crystal Lattices* (Oxford University Press, 1998).
[2]J. J. Rehr and R. C. Albers, Rev. Mod. Phys. **72**, 621 (2000).
[3]G. Bunker, *Introduction to XAFS* (Cambridge University Press, Cambridge, 2010).
[4]G. Beni and P. M. Platzman, Phys. Rev. B **14**, 1514 (1976).
[5]E. Sevillano, H. Meuth, and J. J. Rehr, Phys. Rev. B **20**, 4908 (1979).
[6]P. Eisenberger and G. S. Brown, Solid State Commun. **29**, 481 (1979).
[7]G. Bunker, Nucl. Instrum. Methods Phys. Res. **207**, 437 (1983).
[8]E. D. Crozier, J. J. Rehr, and R. Ingalls, in *X-ray Absorption*, edited by D. C. Koningsberger, and R. Prins (John Wiley & Sons, New York, 1988), Chap. 9, pp. 373–442.
[9]G. Dalba, P. Fornasini, R. Grisenti, and J. Purans, Phys. Rev. Lett. **82**, 4240 (1999).
[10]P. Fornasini, S. a Beccara, G. Dalba, R. Grisenti, A. Sanson, M. Vaccari, and F. Rocca, Phys. Rev. B **70**, 174301 (2004).
[11]S. a Beccara, G. Dalba, P. Fornasini, R. Grisenti, F. Rocca, and A. Sanson, Nucl. Instrum. Methods Phys. Res. B **200**, 237 (2003).
[12]N. Abd el All, G. Dalba, D. Diop, P. Fornasini, R. Grisenti, O. Mathon, F. Rocca, B. Thiodjio Sendja, and M. Vaccari, J. Phys.: Condens. Matter **24**, 115403 (2012).
[13]J. Purans, N. D. Afify, G. Dalba, R. Grisenti, S. De Panfilis, A. Kuzmin, V. I. Ozhogin, F. Rocca, A. Sanson, S. I. Tiutiunnikov, and P. Fornasini, Phys. Rev. Lett. **100**, 055901 (2008).
[14]G. Dalba, D. Diop, P. Fornasini, and F. Rocca, J. Phys.: Condens. Matter **6**, 3599 (1994).
[15]F. D. Vila, J. J. Rehr, H. H. Rossner, and H. J. Krappe, Phys. Rev. B **76**, 014301 (2007).
[16]M. Vaccari, R. Grisenti, P. Fornasini, F. Rocca, and A. Sanson, Phys. Rev. B **75**, 184307 (2007).
[17]C. S. Schnohr, P. Kluth, L. L. Araujo, D. J. Sprouster, A. P. Byrne, G. J. Foran, and M. C. Ridgway, Phys. Rev. B **79**, 195203 (2009).
[18]N. Abd el All, B. Thiodjio Sendja, R. Grisenti, F. Rocca, D. Diop, O. Mathon, S. Pascarelli, and P. Fornasini, J. Synchrotron Radiat. **20**, 603 (2013).
[19]A. Di Cicco, G. Aquilanti, M. Minicucci, E. Principi, N. Novello, A. Cognigni, and L. Olivi, J. Phy.: Conf. Ser. **190**, 012043 (2009).
[20]J. M. Tranquada and R. Ingalls, Phys. Rev. B **28**, 3520 (1983).
[21]G. Dalba, P. Fornasini, and F. Rocca, Phys. Rev. B **47**, 8502 (1993).
[22]J. J. Rehr, S. I. Zabinsky, and R. C. Albers, Phys. Rev. Lett. **69**, 3397 (1992).
[23]A. L. Ankudinov, B. Ravel, J. J. Rehr, and S. D. Conradson, Phys. Rev. B **58**, 7565 (1998).
[24]M. Newville, J. Synchrotron Radiat. **8**, 322 (2001).
[25]B. Ravel and M. Newville, J. Synchrotron Radiat. **12**, 537 (2005).
[26]T. F. Smith and G. K. White, J. Phys. C **8**, 2031 (1975).
[27]S. I. Novikova, Sov. Phys. Solid State **2**, 2087 (1961).
[28]M. Leszczynski, V. B. Pluzhnikov, A. Czopnik, J. Bak-Misiuk, and T. Slupinski, J. Appl. Phys. **82**, 4678 (1997).
[29]P. Fornasini, e-J. Surf. Sci. Nanotechnol. **10**, 480 (2012).
[30]M. Vaccari and P. Fornasini, J. Synchrotron Radiat. **13**, 321 (2006).
[31]A. I. Frenkel and J. J. Rehr, Phys. Rev. B **48**, 585 (1993).
[32]T. Yokoyama, J. Synchrotron Radiat. **6**, 323 (1999).
[33]J. S. Reid, Acta Crystallogr., Sect. A: Found. Crystallogr. **39**, 1 (1983).
[34]S. a Beccara and P. Fornasini, Phys. Rev. B **77**, 172304 (2008).
[35]T. Yokoyama and K. Eguchi, Phys. Rev. Lett. **107**, 065901 (2011).
[36]A. Sanson, Phys. Rev. B **81**, 012304 (2010).
[37]N. Van Hung and P. Fornasini, J. Phys. Soc. Jpn. **76**, 084601 (2007).
[38]R. M. Martin, Phys. Rev. B **1**, 4005 (1970).
[39]S. I. Ahmed, G. Dalba, P. Fornasini, M. Vaccari, F. Rocca, A. Sanson, J. Li, and A. W. Sleight, Phys. Rev. B **79**, 104302 (2009).
[40]P. N. Keating, Phys. Rev. **145**, 637 (1966).
[41]E. A. Stern, P. Livins, and Z. Zhang, Phys. Rev. B **43**, 8850 (1991).
[42]G. K. White, Contemp. Phys. **34**, 193 (1993).
[43]G. D. Barrera, J. A. Bruno, T. H. K. Barron, and N. L. Allan, J. Phys.: Condens. Matter **17**, R217 (2005).
[44]T. A. Mary, J. S. O. Evans, T. Vogt, and A. W. Sleight, Science **272**, 90 (1996).
[45]A. Sanson, F. Rocca, G. Dalba, P. Fornasini, R. Grisenti, M. Dapiaggi, and G. Artioli, Phys. Rev. B **73**, 214305 (2006).
[46]S. Adachi, *GaAs and Related Materials* (World Scientific, 1999).
[47]C. H. Booth, F. Bridges, E. D. Bauer, G. G. Li, J. B. Boyce, T. Claeson, C. W. Chu, and Q. Xiong, Phys. Rev. B **52**, R15745 (1995).
[48]I. K. Jeong, R. H. Heffner, M. J. Graf, and S. J. L. Billinge, Phys. Rev. B **67**, 104301 (2003).
[49]C. J. Martin and D. A. O'Connor, J. Phys. C **10**, 3521 (1977).
[50]J. T. Day, J. G. Mullen, and R. Shukla, Phys. Rev. B **52**, 168 (1995).
[51]R. D. Horning and J. L. Staudenmann, Phys. Rev. B **34**, 3970 (1986).
[52]T. Soma and H. Matsuo, Phys. Status Solidi B **111**, K93 (1982).